The Astrophysical Journal, 661:982–994, 2007 June 1

A SPECTACULAR RADIO FLARE FROM XRF 050416a AT 40 DAYS AND IMPLICATIONS FOR THE NATURE OF X-RAY FLASHES

A. M. Soderberg,[1] E. Nakar,[2] S. B. Cenko,[3] P. B. Cameron,[1] D. A. Frail,[4] S. R. Kulkarni,[1] D. B. Fox,[5] E. Berger,[6,7,8] A. Gal-Yam,[1,8] D-S. Moon,[3] P. A. Price,[9] G. Anderson,[10] B. P. Schmidt,[10] M. Salvo,[10] J. Rich,[10] A. Rau,[1] E. O. Ofek,[1] R. A. Chevalier,[11] M. Hamuy,[6] F. A. Harrison,[3] P. Kumar,[12] A. MacFadyen,[13] P. J. McCarthy,[6] H. S. Park,[14] B. A. Peterson,[10] M. M. Phillips,[6] M. Rauch,[6] M. Roth,[6] and S. Shectman[6]

Received 2006 July 23; accepted 2007 February 5

ABSTRACT

We present detailed optical, near-infrared, and radio observations of the X-ray flash XRF 050416a obtained with Palomar and Siding Springs Observatories, as well as the *HST* and VLA, placing this event among the best-studied X-ray flashes to date. In addition, we present an optical spectrum from Keck LRIS from which we measure the redshift of the burst, $z = 0.6528$. At this redshift the isotropic-equivalent prompt energy release was about 10^{51} ergs, and using a standard afterglow synchrotron model, we find that the blast wave kinetic energy is a factor of 10 larger, $E_{K,\rm iso} \approx 10^{52}$ ergs. The lack of an observed jet break to $t \sim 20$ days indicates that the opening angle is $\theta_j \gtrsim 7^\circ$ and the total beaming-corrected relativistic energy is $\gtrsim 10^{50}$ ergs. We further show that the burst produced a strong radio flare at $t \sim 40$ days accompanied by an observed flattening in the X-ray band, which we attribute to an abrupt circumburst density jump or an episode of energy injection (from either a refreshed shock or off-axis ejecta). Late-time observations with *HST* show evidence for an associated supernova with peak optical luminosity roughly comparable to that of SN 1998bw. Next, we show that the host galaxy of XRF 050416a is actively forming stars at a rate of at least 2 $M_\odot$ yr^{-1} with a luminosity of $L_B \approx 0.5L^*$ and metallicity of $Z \sim 0.2$–$0.8\ Z_\odot$. Finally, we discuss the nature of XRF 050416a in the context of short-hard GRBs and under the framework of off-axis and dirty fireball models for X-ray flashes.

Subject headings: gamma rays: bursts

1. INTRODUCTION

Nearly a decade ago, X-ray flashes (XRFs) were observationally recognized as a subclass within the sample of gamma-ray bursts (GRBs) detected by the *BeppoSAX* Wide Field Cameras (Heise et al. 2001). The events are distinguished by a prompt spectrum that peaks in the soft X-ray range ($E_p \lesssim 25$ keV), a factor of $\sim$10 below the typical values observed for GRBs (Band et al. 1993). Since then, it has been shown that XRFs and GRBs share many observational properties, including prompt emission durations (Sakamoto et al. 2005), redshifts (Soderberg et al. 2004a), broadband afterglows (e.g., XRF 050406; Romano et al. 2006; Schady et al. 2006), and host galaxy properties (Bloom et al. 2003a; Jakobsson et al. 2004; Rau et al. 2005). Moreover, the recent discovery of Type Ic supernovae (SNe) in association with XRF 020903 (Soderberg et al. 2005; Bersier et al. 2006) and XRF 060218 (Pian et al. 2006; Mirabal et al. 2006; Modjaz et al. 2006) indicates that XRFs, like GRBs, are produced in massive stellar explosions. Together, these clues strongly suggest that XRFs and GRBs share similar progenitors.

Driven by this progress, several theories have been proposed to explain the soft prompt emission observed for XRFs under the framework of a standard GRB model. One popular idea posits that XRFs are merely typical GRBs viewed away from the collimation axis (e.g., Yamazaki et al. 2003). In this scenario the prompt emission is primarily beamed away from our line of sight, resulting in lower fluence and E_p values for the observed burst. An important implication of the off-axis model is that the early afterglow evolution should be characterized by a rising phase as the jet decelerates and spreads sideways into our line of sight (Granot et al. 2002; Waxman 2004; Soderberg et al. 2006b).

Another theory suggests that XRFs are intrinsically different from GRBs in their ability to couple energy to highly relativistic material. In this scenario, XRFs are produced in explosions characterized by lower bulk Lorentz factors, $10 \lesssim \Gamma \lesssim 100$, than those inferred for typical GRBs, $\Gamma \gtrsim 100$ (Zhang et al. 2004). This may be the result of baryon loading of the high-velocity ejecta, a so-called dirty fireball (Dermer et al. 1999). Generally speaking, low Lorentz factor explosions may be identified through an analysis of their prompt emission since an optically thin spectrum at high energies implies a lower limit on the Lorentz factor (Lithwick & Sari 2001). In the case of X-ray flashes, however, there are generally insufficient high-energy photons for this type of analysis. For these events, detailed modeling of the broadband afterglow may be used to place a lower limit on the Lorentz factor.

[1] Division of Physics, Mathematics and Astronomy, California Institute of Technology, Pasadena, CA 91125.
[2] Theoretical Astrophysics, California Institute of Technology, Pasadena, CA 91125.
[3] Space Radiation Laboratory, California Institute of Technology, Pasadena, CA 91125.
[4] National Radio Astronomy Observatory, Socorro, NM 87801.
[5] Department of Astronomy and Astrophysics, Pennsylvania State University, University Park, PA 16802.
[6] Observatories of the Carnegie Institution of Washington, Pasadena, CA 91101.
[7] Princeton University Observatory, Princeton, NJ 08544.
[8] Hubble Fellow.
[9] Institute for Astronomy, University of Hawaii, Honolulu, HI 96822.
[10] Research School of Astronomy and Astrophysics, Australian National University, Mount Stromlo Observatory, Weston Creek, ACT 2611, Australia.
[11] Department of Astronomy, University of Virginia, Charlottesville, VA 22903-0818.
[12] Astronomy Department, University of Texas, Austin, TX 78731.
[13] Institute for Advanced Study, Princeton, NJ 08540.
[14] Lawrence Livermore National Laboratory, Livermore, CA 94550.

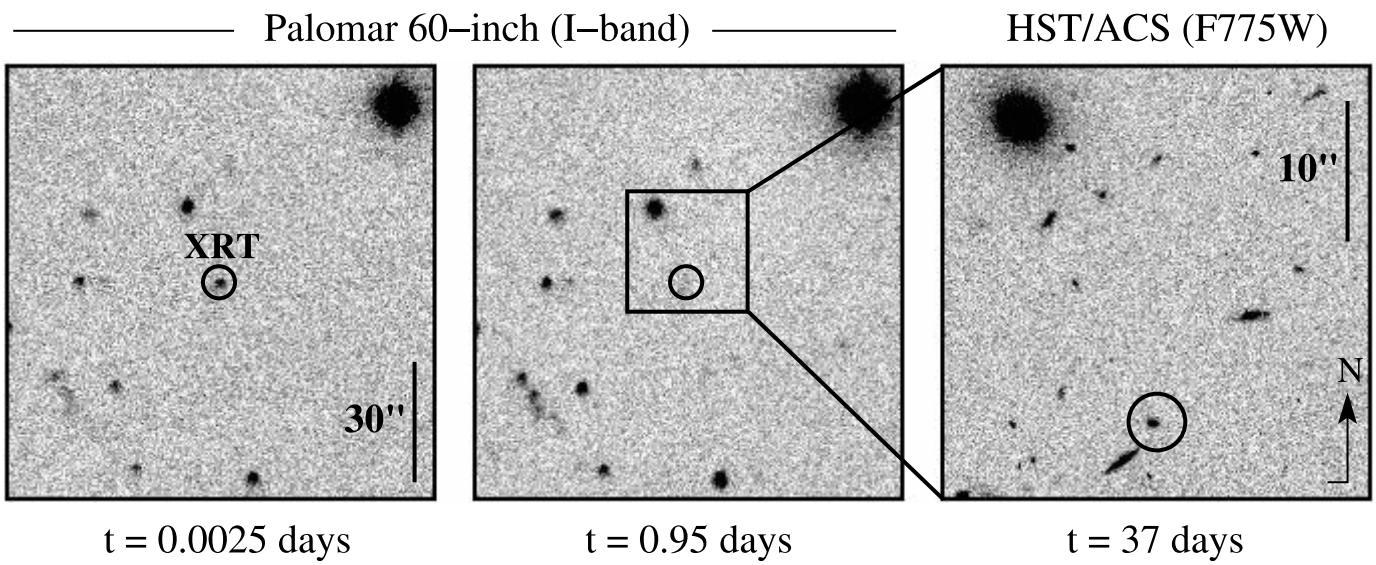

FIG. 1.—Discovery image of the afterglow of XRF 050416a. We began observing the field of XRF 050416a with the Palomar 60 inch telescope in the *I* band about 2.5 minutes after the burst. We discovered a fading source within the 3.0′ (radius) *Swift* BAT error circle. Subsequent localizations of the XRT (*open circle*) and UVOT afterglow positions were shown to be coincident with the P60 source. Our late-time *HST* images reveal a host galaxy coincident with the optical afterglow position.

Here we present an extensive, multifrequency data set for XRF 050416a at $z = 0.6528$ that extends to $t \sim 220$ days after the burst. By combining near-infrared (NIR), optical, ultraviolet, radio and X-ray data, we present an in-depth analysis of the afterglow, energetics, supernova, and host galaxy of XRF 050416a, placing it among the best-studied X-ray flashes to date. Moreover, thanks to our dedicated late-time monitoring campaign, we show that XRF 050416a produced a strong radio flare at $t \sim 40$ days accompanied by a brief plateau phase in the X-ray band. Finally, we discuss the nature of XRF 050416a in the context of off-axis and dirty fireball models for X-ray flashes.

2. OBSERVATIONS

XRF 050416a was discovered by the *Swift* Burst Alert Telescope (BAT) on 2005 April 16.4616 UT. The ratio of 15–25 keV and 25–50 keV channel fluences, $f_{15\text{–}25\ \mathrm{keV}}/f_{25\text{–}50\ \mathrm{keV}} \approx 1.1$, classifies the event as an X-ray flash (Sakamoto et al. 2006a). This is consistent with the low peak photon energy, $E_p = 15.0^{+2.3}_{-2.7}$ keV (Sakamoto et al. 2006a), a factor of ~10 lower than the typical values observed for long-duration GRBs (Band et al. 1993), and a factor of ~3 larger than the values inferred for XRF 020903 and XRF 060218 (Sakamoto et al. 2004; Campana et al. 2006).

As discussed by Sakamoto et al. (2006a), the prompt emission light curve is characterized by a relatively smooth, triangular peak that is only detected at energies below 50 keV. The burst duration is $T_{90} \approx 2.4$ s (15–150 keV), placing it between the classes of short- and long-duration GRBs, while the hardness ratio shows a clear softening. In addition, Sakamoto et al. (2006a) note two intriguing features of the data: (1) the rise time of the pulse is longer than the decay time, and (2) the cross-correlation lag function (an indication of the spectral softening) is $-0.066^{+0.014}_{-0.018}$ s, apparently inconsistent with the overall softening trend observed for the light curves. This lag function estimate is significantly different than the typical values inferred for long-duration GRBs and even more extreme than the zero spectral lags inferred for short-hard bursts (SHBs; Norris & Bonnell 2006). We note, however, that the spectral lag for XRF 050416a was derived through a comparison of the two softest BAT bands (15–25 and 25–50 keV) and therefore prevents a clear comparison with the spectral lag estimates for other *Swift* GRBs for which 15–25 and 50–100 keV bands are typically used. Given that the temporal evolution is not strongly variable, this may indicate that the prompt emission was produced by another process (e.g., external shocks; Dermer et al. 1999). Finally, we note that this burst is inconsistent with the lag-luminosity correlation for long-duration GRBs that posits that low-luminosity bursts such as XRF 050416a have long spectral lags (Norris et al. 2000).

2.1. *Early Optical Observations*

Using the roboticized Palomar 60 inch (1.5 m) telescope (P60), we initiated observations of the field of XRF 050416a at 2005 April 16.4634 UT (2.5 minutes after the burst). In our first 120 s image we discovered a new source within the *Swift* BAT error circle at $\alpha = 12^{\mathrm{h}}33^{\mathrm{m}}54.58^{\mathrm{s}}$, $\delta = +21^{\circ}03'26.7''$ (J2000.0) with an uncertainty of $0.5''$ in each coordinate based on an astrometric tie to the USNO-B catalog (Fig. 1). We subsequently monitored the afterglow evolution with the Palomar 60 inch, 200 inch (5.08 m), and Siding Springs 2.3 m telescopes in the *R*, *I*, z', and K_s bands through $t \approx 7$ days.

Aperture photometry was performed on each of the images in the standard method using the APPHOT package within IRAF. Absolute calibration of *R*-, *I*-, and z'-band light curves was derived using the field calibration of Henden (2005) and utilizing the transformation equations of Smith et al. (2002). The K_s-band light curve was calibrated against the Two Micron All Sky Survey (2MASS) using 15 unconfused sources. The errors resulting from calibration uncertainty ($\lesssim$10%) were added in quadrature to the measurement errors. As shown in Figure 2 and Table 1, the afterglow was $I = 18.82 \pm 0.11$ mag at $t \approx 1.6$ minutes (midexposure).

We supplement these NIR/optical afterglow data with additional measurements from the GCNs (Li et al. 2005; Price et al. 2005; Qiu et al. 2005; Torii 2005; Yanagisawa et al. 2005) and those reported by Holland et al. (2007) obtained with the *Swift* UVOT and 1.54 m Danish Telescope. The resulting data set spans the range from 1930 (*Swift* UVOT UVW2) to 22000 Å (K_s); however, we note that the majority of the UV observations are upper limits. Using this extended data set, we measure the temporal

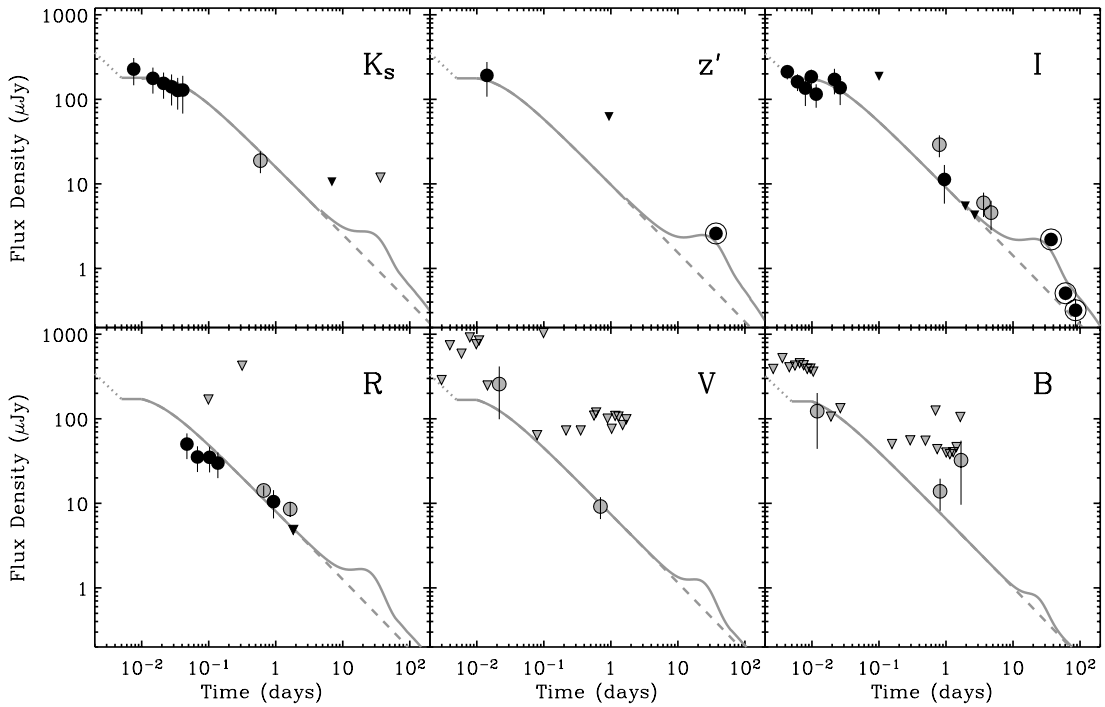

FIG. 2.—Optical (*BVRIz′*) and NIR (K_s) light curves of the afterglow of XRF 050416a. We supplement our measurements from Table 1 (*black symbols*) with data from the GCNs (Li et al. 2005; Price et al. 2005; Qiu et al. 2005; Torii 2005; Yanagisawa et al. 2005) and Holland et al. (2007) (*gray symbols*). Detections are shown as circles and upper limits as inverted triangles. *R*-band data from the ANU 2.3 m have been binned for clarity. All data have been corrected for host galaxy extinction (see § 2.1). Between $t \approx 0.01$ and 1 days the NIR/optical afterglow shows an average decay index of $\overline{\alpha}_{\rm NIR/opt} \approx -0.75$. As described in § 3.2, we find a reasonable fit to the spectral and temporal evolution of the broadband data with a standard afterglow model. Our *HST* measurements are shown as encircled dots; the implied steep spectral index suggests the contribution from an SN component at $t \sim 40$ days (§ 4.4). We sum the flux from an SN 1998bw–like SN at $z = 0.6528$ with our afterglow model to produce the final fits (*solid gray lines*). For comparison, we also show the afterglow model alone (*dashed gray line*). We note that this model does not apply to the very early afterglow evolution at $t \lesssim 0.01$ days. The dotted gray lines at early time represent the evolution of the NIR/optical assuming that these bands track the X-ray evolution on this timescale.

and spectral properties of the NIR/optical afterglow emission. We find the following NIR/optical power-law decay indices (α, where $F_\nu \propto t^\alpha$) between ~0.01 and 1 days: $\alpha_{K_s} = -0.7 \pm 0.3$, $\alpha_I = -0.7 \pm 0.3$, $\alpha_R = -0.5 \pm 0.3$, $\alpha_V = -1.0 \pm 0.3$, $\alpha_B = -0.5 \pm 0.3$, consistent with the values reported by Holland et al. (2007). These values imply a mean temporal index of $\overline{\alpha}_{\rm NIR/opt} = -0.7 \pm 0.2$.

Finally, we analyze the spectral index (β with $F_\nu \propto \nu^\beta$) within the NIR/optical bands. As shown in Figure 3, there are two epochs at which the photometric spectrum is well sampled: $t \approx 0.014$ and 0.8 days. We fit each of the observed spectra with a simple power law and find $\beta_{\rm NIR/opt} \approx -1.3$ ($\chi^2_r \approx 0.5$) and -1.5 ($\chi^2_r \approx 0.6$) for the first and second epochs, respectively. As discussed in § 3.1, the observed steep spectrum is indicative of extinction within the host galaxy.

2.2. *Late-Time Observations with HST*

Using the Wide Field Camera (WFC) of the Advanced Camera for Surveys (ACS) on board the *Hubble Space Telescope* (*HST*), we imaged the field of XRF 050416a four times, spanning 37–219 days after the burst. Each epoch consisted of two or four orbits during which we imaged the field in filters F775W and/or F850LP, corresponding to SDSS i' and z' bands, respectively.

The *HST* data were processed using the `multidrizzle` routine (Fruchter & Hook 2002) within the STSDAS package of IRAF. Images were drizzled using `pixfrac` = 0.8 and `pixscale` = 1.0, resulting in a final pixel scale of $0.05''$ pixel^{-1}. Drizzled images were then registered to the final epoch using the XREGISTER package within IRAF. We astrometrically tied the *HST* and P60 images using 12 unconfused sources in common, resulting in a final systematic uncertainty of $0.70''$ ($2\,\sigma$).

To search for source variability and remove host galaxy contamination, we used the ISIS subtraction routine by Alard (2000), which accounts for temporal variations in the stellar point-spread function. Adopting the final-epoch observations as templates, we produced residual images. These residual images were examined for positive sources positionally coincident with the P60 afterglow.

Photometry was performed on the residual sources within a $0.5''$ aperture. We converted the photometric measurements to infinite aperture and calculated the corresponding AB magnitudes within the native *HST* filters using the aperture corrections and zero points provided by Sirianni et al. (2005). Here we made the reasonable assumption that the transient flux is negligible in the template images. For comparison with ground-based data, we also converted the F775W measurements to Johnson *I*-band (Vega) magnitudes using the transformation coefficients derived by Sirianni et al. (2005) and assuming the F_ν source spectrum implied by the first-epoch *HST* data.

As shown in Table 2 and Figure 4, the transient is clearly detected in the first-epoch *HST* residual images. An astrometric tie between the first and final epochs shows that the residual is offset $0.02'' \pm 0.02''$ from the center of the host galaxy. Our residual images show the source to be F775W = 24.35 ± 0.02 mag and F850LP = 23.83 ± 0.03 mag in the AB system ($I = 23.82 \pm 0.02$ mag in the Vega system) at $t \approx 37$ days. As shown in Figure 2, these values are a factor of ~5 above an extrapolation of the early afterglow decay. The observed spectral index between the F775W and F850LP filters is $\beta_{HST} \approx -2.8 \pm 0.3$, significantly steeper than the afterglow spectrum observed at early time (§ 2.1 and Fig. 3), as well as the typical values measured for NIR/optical afterglows ($\beta_{\rm NIR/opt} \approx -0.6$; Panaitescu

TABLE 1
GROUND-BASED OPTICAL AND NIR OBSERVATIONS OF XRF 050416a

Date Observed (UT)	Δt[a] (days)	Telescope	Filter	Magnitude[b]
2005 Apr 16.4641	0.0025	Palomar 60 inch	I	18.82 ± 0.11
2005 Apr 16.4659	0.0043	Palomar 60 inch	I	18.86 ± 0.11
2005 Apr 16.4677	0.0061	Palomar 60 inch	I	19.16 ± 0.13
2005 Apr 16.4696	0.0080	Palomar 60 inch	I	19.35 ± 0.23
2005 Apr 16.4692	0.0076	Palomar 200 inch	K_s	16.37 ± 0.21
2005 Apr 16.4714	0.0098	Palomar 60 inch	I	19.01 ± 0.12
2005 Apr 16.4731	0.0116	Palomar 60 inch	I	19.53 ± 0.18
2005 Apr 16.4772	0.0156	Palomar 60 inch	z'	19.16 ± 0.27[c]
2005 Apr 16.4763	0.0147	Palomar 200 inch	K_s	16.64 ± 0.20
2005 Apr 16.4833	0.0217	Palomar 60 inch	I	19.09 ± 0.20
2005 Apr 16.4828	0.0212	Palomar 200 inch	K_s	16.79 ± 0.20
2005 Apr 16.4880	0.0264	Palomar 60 inch	I	19.34 ± 0.23
2005 Apr 16.4895	0.0279	Palomar 200 inch	K_s	16.89 ± 0.24
2005 Apr 16.4960	0.0344	Palomar 200 inch	K_s	16.99 ± 0.25
2005 Apr 16.5026	0.0410	Palomar 200 inch	K_s	16.98 ± 0.29
2005 Apr 16.5089	0.0473	ANU 2.3 m	R	20.92 ± 0.05
2005 Apr 16.5502	0.0886	ANU 2.3 m	R	21.18 ± 0.12
2005 Apr 16.5543	0.0927	ANU 2.3 m	R	21.40 ± 0.15
2005 Apr 16.5585	0.0969	ANU 2.3 m	R	21.16 ± 0.08
2005 Apr 16.5626	0.1010	ANU 2.3 m	R	21.43 ± 0.11
2005 Apr 16.5669	0.1053	ANU 2.3 m	R	21.44 ± 0.26
2005 Apr 16.5702	0.1086	ANU 2.3 m	R	21.39 ± 0.16
2005 Apr 16.5744	0.1128	ANU 2.3 m	R	21.37 ± 0.16
2005 Apr 16.5779	0.1163	ANU 2.3 m	R	21.18 ± 0.17
2005 Apr 16.5816	0.1200	ANU 2.3 m	R	21.35 ± 0.16
2005 Apr 16.5850	0.1234	ANU 2.3 m	R	21.36 ± 0.10
2005 Apr 16.5893	0.1277	ANU 2.3 m	R	21.44 ± 0.27
2005 Apr 16.5924	0.1308	ANU 2.3 m	R	21.46 ± 0.22
2005 Apr 16.5975	0.1359	ANU 2.3 m	R	21.63 ± 0.34
2005 Apr 16.6092	0.1476	ANU 2.3 m	R	21.71 ± 0.30
2005 Apr 16.6187	0.1571	ANU 2.3 m	R	21.87 ± 0.46
2005 Apr 17.3895	0.9279	Palomar 60 inch	R	22.62 ± 0.30
2005 Apr 17.4006	0.9390	Palomar 60 inch	z'	<20.38[c]
2005 Apr 17.4087	0.9467	Palomar 60 inch	I	22.05 ± 0.30
2005 Apr 18.2884	1.8264	Palomar 60 inch	R	<23.46
2005 Apr 18.4031	1.9411	Palomar 60 inch	I	<22.83
2005 Apr 23.3511	6.8896	Palomar 200 inch	K_s	<19.70

[a] Days since explosion have been calculated for the midpoint of each exposure.
[b] Magnitudes have not been corrected for extinction. Limits are given as 3 σ.
[c] AB system.

& Kumar 2002; Yost et al. 2003). As discussed in § 4.4, the timescale and spectral signature of the observed flux excess are suggestive of a thermal SN component.

2.3. *Spectroscopic Observations*

We observed the host galaxy of XRF 050416a with the Low Resolution Imaging Spectrometer (LRIS) on Keck I on 2005 June 6.3 UT ($t \sim 50$ days). We placed a 1.0″ long slit across the host galaxy at a position angle of P.A. = 87°. Data were reduced in standard manner using the ONEDSPEC and TWODSPEC packages within IRAF. Flux calibration was performed using the spectrophotometric standard star BD +28 4211.

As shown in Figure 5 and Table 3, we detect several strong emission lines in the spectrum including Hβ, Hγ, [O II] λ3727, and [O III] $\lambda\lambda$4959, 5006 at a redshift of $z = 0.6528 \pm 0.0002$. Adopting the standard cosmological parameters ($H_0 = 71$ km s^{-1} Mpc^{-1}, $\Omega_M = 0.27$, $\Omega_\Lambda = 0.73$), the isotropic gamma-ray energy release is $E_{\gamma,\rm iso} \approx (1.2 \pm 0.2) \times 10^{51}$ ergs (1 keV–10 MeV; Sakamoto et al. 2006a). Compared with typical long-duration bursts, the prompt energy release of XRF 050416a is a factor of ~100 lower (Frail et al. 2001; Bloom et al. 2003b; Amati 2006 and references therein).

2.4. *Radio Observations*

We began observing XRF 050416a with the Very Large Array[15] (VLA) on 2005 April 16.49 UT ($t \approx 37$ minutes). No radio source was detected coincident with the optical position to a limit of $F_\nu < 122$ μJy at $\nu = 8.46$ GHz. However, further observations at $t \approx 5.6$ days revealed a new radio source with $F_\nu \approx 101 \pm 34$ μJy coincident with the optical and X-ray afterglow positions at $\alpha = 12^{\rm h}33^{\rm m}54.594^{\rm s} \pm 0.002^{\rm s}$, $\delta = 21^\circ 03' 26.27'' \pm 0.04''$ (J2000.0), which we identify as the radio afterglow.

We continued to monitor the radio afterglow at 1.43, 4.86, and 8.46 GHz through $t \approx 140$ days (Table 4). All observations were taken in standard continuum observing mode with a bandwidth of 2×50 MHz. We used 3C 286 (J1331+305) for flux

[15] The Very Large Array and Very Long Baseline Array are operated by the National Radio Astronomy Observatory, a facility of the National Science Foundation operated under cooperative agreement by Associated Universities, Inc.

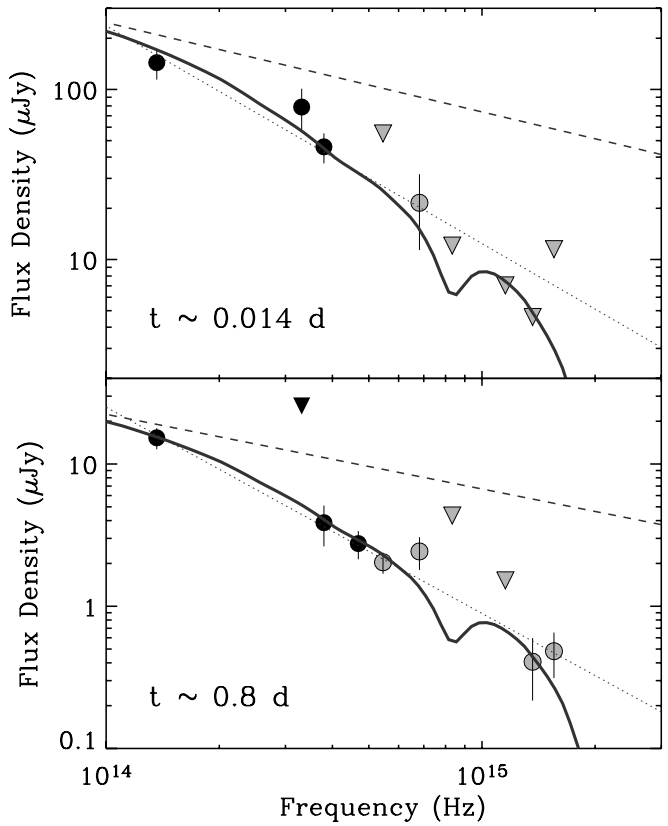

FIG. 3.—Observed photometric spectrum for XRF 050416a at $t \approx 0.014$ (*top*) and 0.8 days (*bottom*). The K_s, z'-, I-, and R-band data (*black symbols*) are from Table 1, while the V, B, U, UVW1, UVM2, and UVW2 data (*gray symbols*) are from Holland et al. (2007) . Detections are shown as circles and upper limits as inverted triangles. The observed spectrum is fitted by $\beta_{\rm NIR/opt} \approx -1.3$ and -1.5 in the top and bottom panels, respectively (*dotted line*). We fit the data with an extinction model (*solid line*), which includes $E(B-V) = 0.03$ from the Galaxy (Schlegel et al. 1998) and a rest-frame host galaxy extinction of $E(B-V)_{\rm rest} = 0.28$ assuming an intrinsic spectral index of $\beta_{\rm NIR/opt} \approx -0.55$ (*dashed line*).

calibration, while phase referencing was performed against calibrators J1221+282 and J1224+213. The data were reduced using standard packages within the Astronomical Image Processing System (AIPS).

As shown in Figure 6, the evolution of the radio afterglow is dissimilar from those of typical GRBs and inconsistent with a standard blast wave model. Between $t \sim 20$ and 40 days an abrupt rebrightening (factor of $\sim$3) is observed at all radio bands with a temporal index steeper than $\alpha_{\rm rad} \approx 0.9$. Following this radio flare the emission decays rapidly with an index of $\alpha_{\rm rad} \lesssim -1.5$. The peak radio luminosity at 8.46 GHz, $L_{\rm rad} \approx 1.3 \times 10^{31}$ ergs s^{-1} Hz^{-1}, is typical for GRBs (Frail et al. 2003), a factor of $\sim$10 and 10^3 larger than those of XRF 020903 and XRF 060218, respectively (Soderberg et al. 2004a, 2006e), and between 10^2 and 10^6 times higher than the peak radio luminosities observed for optically selected Type Ibc SNe (Soderberg 2006). By $t \approx 105$ days the radio afterglow is no longer detected at any frequency.

2.5. *X-Ray Observations*

The afterglow of XRF 050416a was observed with the *Swift* X-Ray Telescope (XRT) beginning 1.2 minutes after the burst and continuing through $t \sim 69$ days, placing it among the best-studied X-ray afterglows to date (Nousek et al. 2006; O'Brien et al. 2006). From their analysis of the XRT data, Mangano et al. (2007) report a spectral index of $\beta_{\rm X} = -1.04^{+0.11}_{-0.05}$ and evidence for significant absorption in the host galaxy, $N_{\rm H} = 6.8^{+1.0}_{-1.2} \times 10^{21}$ cm^{-2}, corresponding to $E(B-V)_{\rm rest} = 1.2 \pm 0.2$ assuming the conversion of Predehl & Schmitt (1995) and a Milky Way extinction curve (Pei 1992). As shown in Figure 7, at $t = 10$ hr the X-ray luminosity was $L_{\rm X,iso}(t = 10\ {\rm hr}) \approx 2.3 \times 10^{45}$ ergs s^{-1}, placing it at the lower edge of the observed distribution for GRBs (Berger et al. 2003b; Freedman & Waxman 2001).

As discussed by Mangano et al. (2007) and shown in Figure 7, the early evolution of the X-ray afterglow can be characterized by three phases: (1) an initial steep decay, (2) a flattening between $t \approx 7$ and 20 minutes during which the flux is roughly constant, and (3) a resumed decay through $t \sim 20$ days. These three phases have been shown to be ubiquitous among *Swift* X-ray afterglows (Nousek et al. 2006). However, at $t \sim 20$ days there is a second flattening that continues through $t \sim 40$ days. By 70 days the X-ray afterglow is no longer detected, implying a significant steepening to $\alpha_{\rm X} \lesssim -1.8$ between the last two observations. We note that the timescale for the X-ray flattening and subsequent steep decay is coincident with the observed radio flare.

3. PROPERTIES OF THE EARLY AFTERGLOW

Using the detailed multifrequency observations of the XRF 050416a afterglow, we can constrain the physical properties of the ejecta and the circumburst density. We adopt a standard relativistic blast wave model in which the afterglow emission is produced through the dynamical interaction of the ejecta with the surrounding medium (the forward shock) with an additional component from shock heating of the ejecta (the reverse shock). In this scenario, the total energy density is partitioned between relativistic electrons, ϵ_e, and magnetic fields, ϵ_B, while the thermal energy of the shocked protons accounts for the fraction remaining (for a review see Piran 1999). The shocked electrons are

TABLE 2
HST ACS OBSERVATIONS OF XRF 050416a

Date Observed (UT)	Δt (days)	Exposure Time (s)	Filter	*HST* Magnitude[a] (AB)	Johnson Magnitude[b] (Vega)
2005 May 23.38.....	36.92	3282	F775W	24.35 ± 0.02	23.82 ± 0.02
2005 May 23.46.....	37.00	3430	F850LP	23.83 ± 0.03	...
2005 Jun 16.17	60.71	3986	F775W	25.88 ± 0.10	25.36 ± 0.10
2005 Jul 11.15	85.69	4224	F775W	26.44 ± 0.22	25.92 ± 0.22
2005 Nov 21.06.....	218.60	4224	F850LP	...	...
2005 Nov 21.19.....	218.73	4224	F775W	...	...

[a] AB system magnitudes in the *HST* filters given in the fourth column. Photometry was done on residual images (see § 2.2). We have assumed the source flux to be negligible in the final (template) epoch. Magnitudes have not been corrected for extinction.

[b] We convert the F775W magnitudes in the fifth column to Johnson I band (Vega system) as described in § 2.2. Magnitudes have not been corrected for extinction.

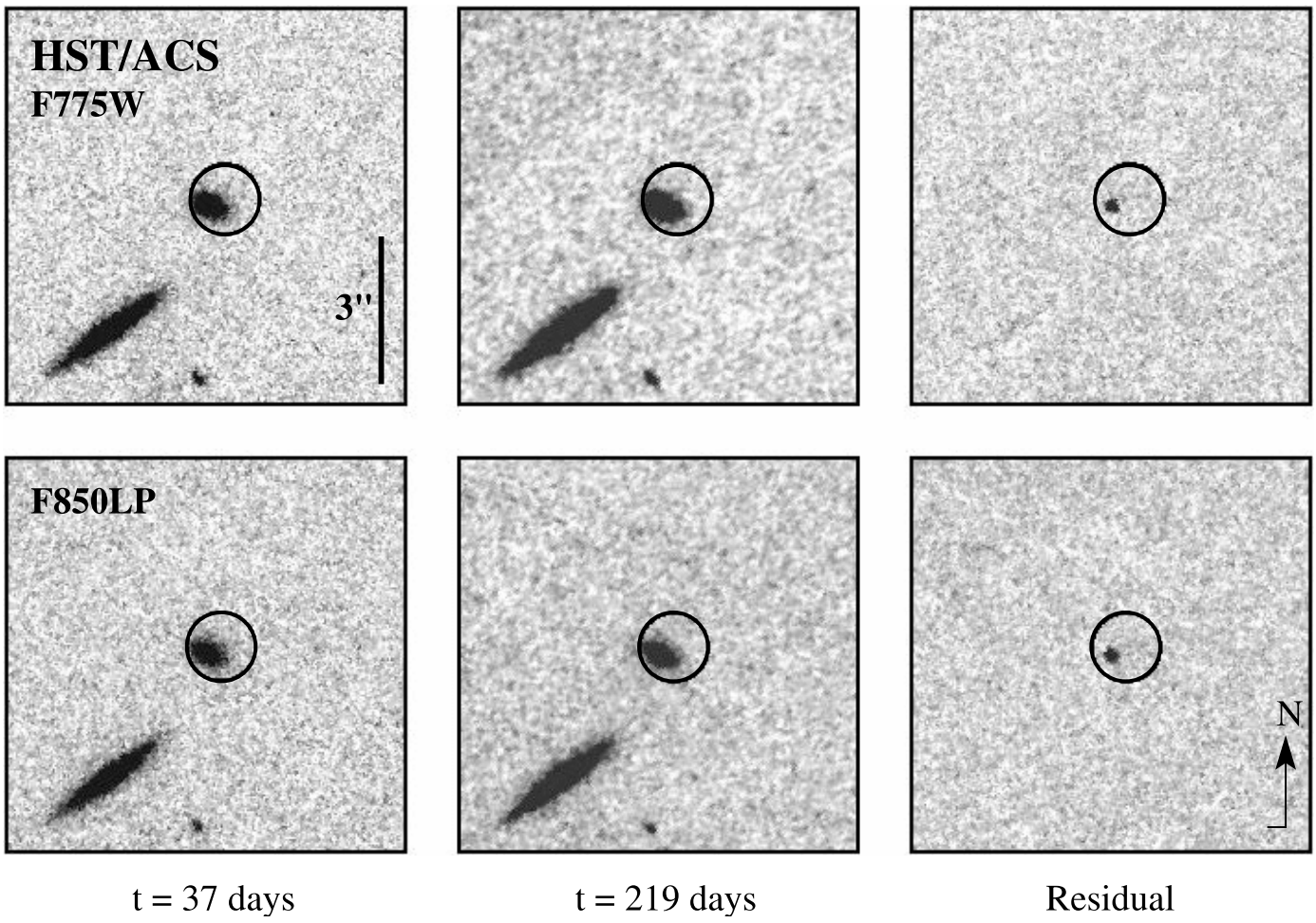

FIG. 4.—*HST* images of XRF 050416a obtained with ACS in filters F775W and F850LP spanning $t \approx 37$–219 days after the explosion. The host galaxy emission dominates that of the afterglow throughout this timescale. Relative astrometry between the P60 and the *HST* images provides an optical afterglow position accurate to $0.70''$ (*open circle*; 2 σ). Residual images of the afterglow were produced through image subtraction techniques (§ 2.2). The position of the afterglow is offset by $0.02'' \pm 0.02''$ with respect to the host galaxy center.

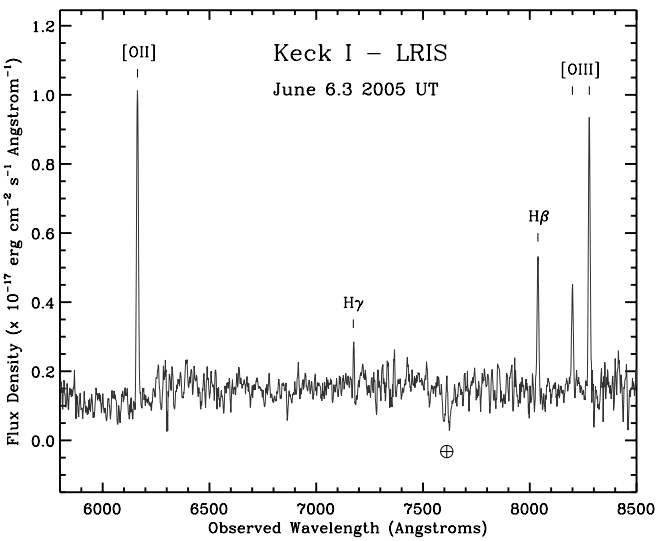

FIG. 5.—Optical spectrum of the host galaxy of XRF 050416a as observed with the LRIS on Keck I on 2005 June 6.3 UT. Several bright emission lines are detected, indicating that the host is a star-forming galaxy at redshift $z = 0.6528 \pm 0.0002$. As discussed in § 5, we find that the host is actively forming stars with a rate of $\gtrsim 2\ M_\odot\ \mathrm{yr}^{-1}$ and an inferred metallicity of $Z \sim 0.2$–$0.8\ Z_\odot$.

accelerated into a power-law distribution, $N(\gamma) \propto \gamma^{-p}$, above a minimum Lorentz factor, γ_m. The emission resulting from the forward and reverse shock components is described by a synchrotron spectrum characterized by three break frequencies (the self-absorption frequency ν_a, the characteristic frequency ν_m, and the cooling frequency ν_c) and a flux normalization, F_{ν_m} (Sari et al. 1998). In modeling the afterglow spectral and temporal evolution, we adopt the formalism of Granot & Sari (2002) for a relativistic forward shock expanding into a constant density circumburst medium.

3.1. *Preliminary Constraints*

In fitting the forward shock model to the afterglow data of XRF 050416a we use only observations between 0.014 and 20 days when the afterglow follows a simple power-law evolution. To constrain the spectrum of the forward shock, we first investigate the afterglow evolution in the optical and X-ray bands. As shown in Figure 7, the X-ray data between 0.014 and 20 days are reasonably fitted with $\alpha_X \approx -1.1$ ($\chi^2_r \approx 0.70$). Mangano et al. (2007) report that the X-ray spectral index on this same timescale is $\beta_X \approx -1.04$, leading to $\alpha - 3\beta/2 \approx 0.5$. A comparison to the standard closure relations, $\alpha - 3\beta/2 = 0$ ($\nu_m < \nu < \nu_c$) and $\alpha - 3\beta/2 = \frac{1}{2}$ ($\nu > \nu_c$), indicates that $\nu_X > \nu_c$. This conclusion is supported by the NIR/X-ray spectral slope, $\beta_{K,X} = -0.47 \pm 0.06$ at $t \approx 0.6$ days, which is flatter than β_X as expected if

TABLE 3
SPECTROSCOPIC LINES FOR XRF 050416a

Line	λ(rest) (Å)	λ(observed)[a] (Å)	Redshift	Flux[b] ($\times 10^{-17}$ ergs cm^{-2} s^{-1})
[O II].....	3728.38	6162.08	0.6528	9.6 ± 0.4
Hγ	4341.72	7174.64	0.6525	1.2 ± 0.2
Hβ	4862.72	8037.14	0.6528	3.7 ± 0.5
[O III].....	4960.30	8198.79	0.6529	2.5 ± 0.3
	5008.24	8277.57	0.6528	8.4 ± 0.4.

[a] Observed wavelengths have been corrected to vacuum.
[b] Flux values have not been corrected for Galactic extinction.

$\nu_{\rm NIR/opt} < \nu_c < \nu_{\rm X}$. Therefore, the X-ray observations suggest that $p = -2\beta \approx 2.1$.

Next we consider the spectral index within the NIR/optical bands. As discussed in § 2.1 and shown in Figure 3, the observed NIR/optical spectral index on this timescale is $\beta_{\rm NIR/opt} \approx -1.3$ to -1.5. These values are significantly steeper than $\beta_{K,\rm X}$ and imply that the optical flux is suppressed by host galaxy extinction. Making the reasonable assumption that $\nu_m \lesssim \nu_{\rm NIR/opt}$ on the timescale of our afterglow observations, and adopting $p \approx 2.1$ as indicated by the X-ray observations, we estimate $\beta_{\rm NIR/opt} = -(p-1)/2 \approx -0.55$ for the intrinsic spectral index of the NIR/optical afterglow. Adopting this value for $\beta_{\rm NIR/opt}$, we find that both NIR/optical spectra are reasonably fitted with a Galactic extinction of $E(B-V) = 0.03$ (Schlegel et al. 1998) and a host galaxy component of $E(B-V)_{\rm rest} \approx 0.28$ (Fig. 3). Here we have assumed a Milky Way extinction model for the host (Pei 1992) but note that a comparable fit may be obtained for an SMC extinction curve. We further note that this optically derived extinction estimate is lower than that inferred from the X-ray spectrum (Mangano et al. 2007), consistent with the trend observed for long-duration GRBs (Galama & Wijers 2001).

With this extinction correction, the NIR/X-ray spectral index becomes $\beta_{K,\rm X} \approx -0.5 \pm 0.1$, consistent with our estimate for the intrinsic spectral index within the NIR/optical band. Moreover, the extinction-corrected NIR/optical spectral index and observed average temporal index of $\overline{\alpha}_{\rm NIR/opt} = -0.7 \pm 0.2$ are consistent with the standard closure relation: $\alpha - 3\beta/2 = 0 \approx 0.1$. We also note that this supports our assumption of a constant density medium since in a wind environment the expected temporal index is steeper than $\alpha = -1.25$ and thus inconsistent with the observed values. Using all the available optical and X-ray observations, we estimate that $\nu_c \approx 1 \times 10^{17}$ Hz at $t = 1$ day.

Next we compare the NIR and radio afterglow data to constrain ν_m and the peak spectral flux, F_{ν_m}. Assuming that ν_m passed through the NIR/optical bands near the time of our first K_s-band observations implies that the peak spectral flux is roughly comparable to the extinction-corrected K_s flux: $F_{K_s} \approx 230$ μJy at $t \approx 11$ minutes. Here we focus on the K_s-band data, since they are the least sensitive to host galaxy extinction, which we estimate to be $A_K \approx 0.24$ mag (a 20% increase in flux) for $E(B-V)_{\rm rest} \approx 0.28$. Scaling these constraints to $t = 1$ day ($\nu_m \propto t^{-1.5}$ and $F_{\nu_m} \propto t^0$) and accounting for the smooth shape of the spectral peak, we find $\nu_m \approx 4.0 \times 10^{11}$ Hz and $F_{\nu_m} \approx 350$ μJy. Here and throughout, F_{ν_m} is the asymptotic extrapolation of the smooth spectrum peak and is therefore slightly higher than the intrinsic peak flux. We note that since the NIR/optical data require $F_{\nu_m} \propto \nu^{-(p-1)/2}$, lower values of ν_m imply increasingly higher values of F_{ν_m} at the time of the first K_s-band observations.

TABLE 4
RADIO OBSERVATIONS OF XRF 050416a

Date Observed (UT)	Δt (days)	$F_{\nu,1.43\ \rm GHz}$[a] (μJy)	$F_{\nu,4.86\ \rm GHz}$ (μJy)	$F_{\nu,8.46\ \rm GHz}$ (μJy)
2005 Apr 16.49.....	0.026	...	...	20 ± 51
2005 Apr 22.03.....	5.57	...	200 ± 46	101 ± 34
2005 Apr 28.29.....	11.83	...	188 ± 42	132 ± 30
2005 May 1.35.....	14.89	...	201 ± 43	...
2005 May 31.10.....	44.64	...	...	431 ± 46
2005 Jun 3.99	48.53	...	585 ± 48	...
2005 Jun 8.03	52.57	420 ± 190	562 ± 51	398 ± 33
2005 Jun 16.97	61.51	...	505 ± 49	330 ± 35
2005 Jun 20.16	64.70	...	...	286 ± 33
2005 Jul 1.92	76.46	843 ± 214	321 ± 48	189 ± 36
2005 Jul 30.02	104.56	0 ± 192	68 ± 36	93 ± 41
2005 Aug 14.97.....	120.51	...	...	72 ± 42
2005 Aug 21.89.....	127.42	...	...	41 ± 47
2005 Sep 19.90.....	156.44	...	0 ± 54	...
2005 Oct 15.73	182.27	...	33 ± 47	89 ± 38

[a] All errors are given as 1 σ (rms).

Finally, we test that these constraints are consistent with the radio observations. Given the evolution of ν_m, these constraints predict that the spectral peak should pass through the radio band at $t \approx 13$ days with an extrapolated peak flux density of $F_{\nu_m} \approx 350$ μJy, roughly consistent with the 4.86 GHz observations on this timescale. We emphasize that the early steady decay of the NIR/optical data requires that ν_m pass through the radio no later than 13 days. Finally, we note that the radio spectrum is optically thin throughout the timescale of VLA monitoring (see Fig. 6), and thus we observationally constrain ν_a to be below 1.43 GHz.

3.2. *Forward Shock Broadband Model*

Adopting these constraints, we apply a broadband afterglow model fit to the multifrequency data in order to determine the physical parameters of the burst. The four spectral parameters (F_{ν_m}, ν_a, ν_m, and ν_c) are fully determined by four physical parameters: the isotropic ejecta energy, $E_{K,\rm iso}$, the energy density partition fractions, ϵ_e and ϵ_B, and the circumburst density, n. Therefore, by constraining the four spectral parameters through broadband observations, we are able to determine a unique solution for the four physical parameters (for reviews see Sari et al. 1998; Piran 1999). Although the radio observations provide only an upper limit on ν_a, we are able to define a range of reasonable values by requiring that $\epsilon_e,\ \epsilon_B \leq \frac{1}{3}$, which accounts for an equal or greater contribution from shocked protons. This requirement excludes unphysical solutions in which the sum of the contributions from shocked electrons, protons, and magnetic fields exceeds the total energy density. Combined with the observed constraints for F_{ν_m}, ν_m, and ν_c, we find the following ranges for the physical parameters:

$$E_{K,\rm iso} \approx (8.2\text{–}14) \times 10^{51}\ \rm ergs, \quad (1a)$$

$$n \approx (0.33\text{–}4.2) \times 10^{-3}\ \rm cm^{-3}, \quad (1b)$$

$$\epsilon_e \approx 0.20\text{–}\tfrac{1}{3}, \quad (1c)$$

$$\epsilon_B \approx 0.072\text{–}\tfrac{1}{3}. \quad (1d)$$

As shown in Figures 2, 6, and 7, this model provides an adequate fit to the broadband data between $t \sim 0.01$ and 20 days.

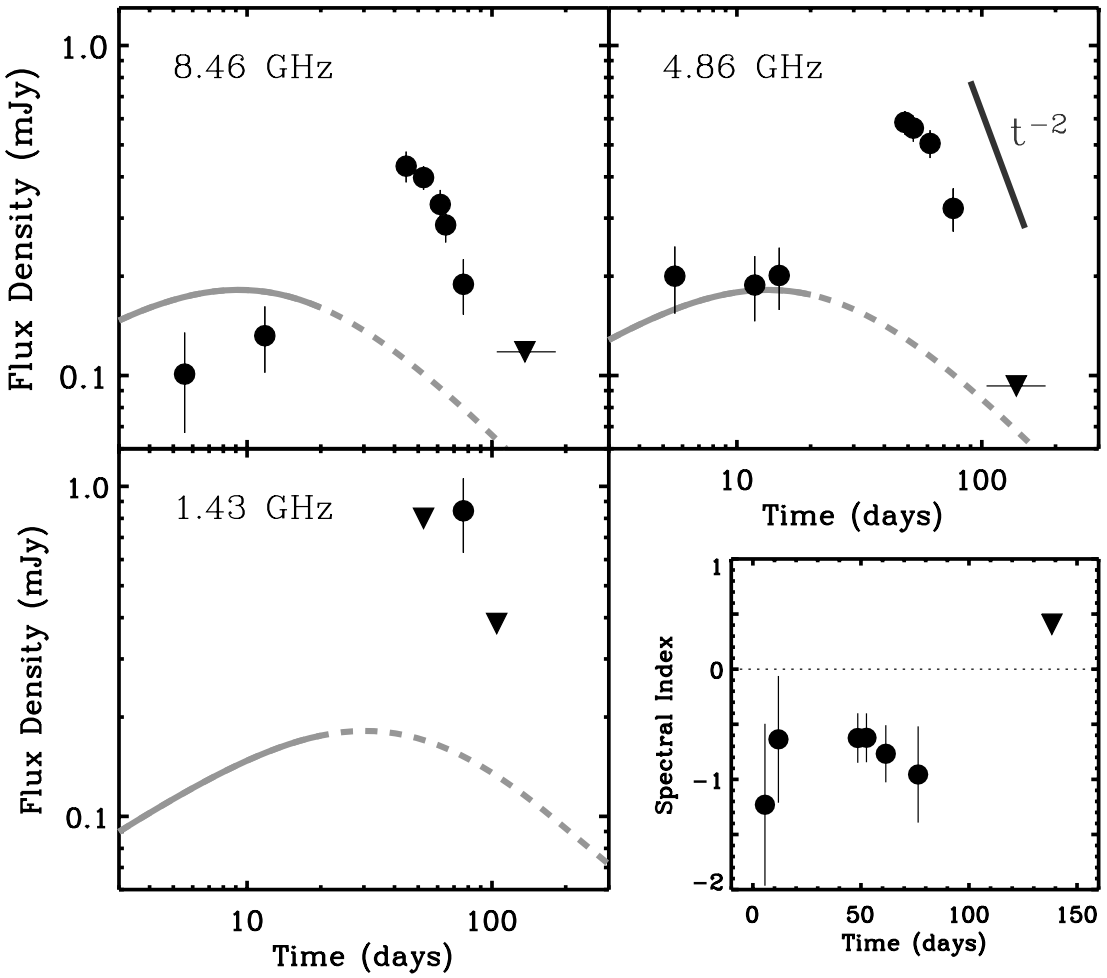

FIG. 6.—Radio observations of XRF 050416a from the VLA as listed in Table 4. We have summed the late-time limits in each frequency for clarity. The radio evolution is characterized by an unusual flare at $t \sim 40$ days, which rapidly fades below our detection limits. This radio flare occurs roughly on the same timescale as the observed X-ray flattening (Fig. 7). We attribute both the radio flare and the X-ray flattening to an episode of late-time energy injection (refreshing shell or off-axis ejecta) or a large circumburst density jump. Our early afterglow model fit is shown (*solid gray lines*) and extrapolated to the epoch of the radio flare (*dashed gray lines*). The spectral index between 8.46 and 4.86 GHz is optically thin throughout our radio monitoring, including the late-time flare (*bottom right panel*).

3.3. *Collimation of the Ejecta and Viewing Angle*

The lack of an observed jet break in the X-rays to $t \sim 20$ days, together with the inferred physical parameters, constrains the opening angle of the jet (e.g., Sari et al. 1999) to $\theta_j \approx 3.1 t_j^{3/8} E_{K,\mathrm{iso},52}^{-1/8} n_{-3}^{1/8} (1+z)^{-3/8} \gtrsim 6.9^\circ$. Here t_j is the jet break time in days and we have adopted the notation $10^x Q_x = Q$. This limit is slightly larger than the median of the jet opening angles inferred for long-duration GRBs, $\theta_j \sim 5^\circ$ (Bloom et al. 2003b; Ghirlanda et al. 2004; Soderberg et al. 2006d and references therein). This indicates that the beaming-corrected ejecta energy release is $E_K \equiv E_{K,\mathrm{iso}}(1-\cos\theta) \approx 9.8 \times 10^{49}$–$1.4 \times 10^{52}$ ergs, where the range includes the uncertainty in $E_{K,\mathrm{iso}}$ and the lower limit on θ_j. Moreover, we expect the blast wave to become nonrelativistic on a timescale $t_{\mathrm{NR}} \approx 2.0 E_{51}^{1/3} n_{-3}^{-1/3} \sim 0.6$–$6.8$ yr (Livio & Waxman 2000). On a similar timescale, the ejecta are predicted to approach spherical symmetry, after which the blast wave evolution is well described by the Sedov–von Neumann–Taylor (SNT) solution (Zel'dovich & Raizer 2002; Frail et al. 2000); in this regime the afterglow emission decays with $\alpha = -9/10$ (-1) for frequencies below (above) the cooling frequency.

Next, the early steady decay of the X-ray and NIR/optical afterglow indicates that the jet collimation axis is directed roughly along our line of sight. In comparison, GRBs viewed significantly off-axis ($\theta_{\mathrm{obs}} > 2\theta_j$) are predicted to show a rising afterglow light curve as the jet spreads sideways and intersects our viewing angle (Granot et al. 2002; Waxman 2004; Soderberg et al. 2006b). Here θ_{obs} is the angle between our line of sight and the jet collimation axis. We conclude that the ejecta are viewed roughly on-axis and therefore the inferred beaming-corrected energies are not affected significantly (if at all) by viewing angle effects.

4. PROPERTIES OF THE LATE-TIME AFTERGLOW

Next we address the nature of the late-time broadband afterglow evolution with special attention to the strong radio flare observed at ~40 days. Radio flares have been noted for several other GRBs, although only at early times (e.g., GRB 990123 at $t \lesssim 1$ day; Kulkarni et al. 1999). Based on their observed timescale and evolution, radio flares are typically attributed to emission from the reverse shock (Sari & Piran 1999). Here we present detailed radio observations for XRF 050416a that show for the first time a strong radio flare at late time. Possible causes for a late-time radio rebrightening include the emission from a decelerating jet initially directed away from our line of sight (Waxman 2004; Li & Song 2004), circumburst density variations (Wijers 2001; Ramirez-Ruiz et al. 2001), and energy injection from a slow shell catching up to and refreshing the afterglow shock

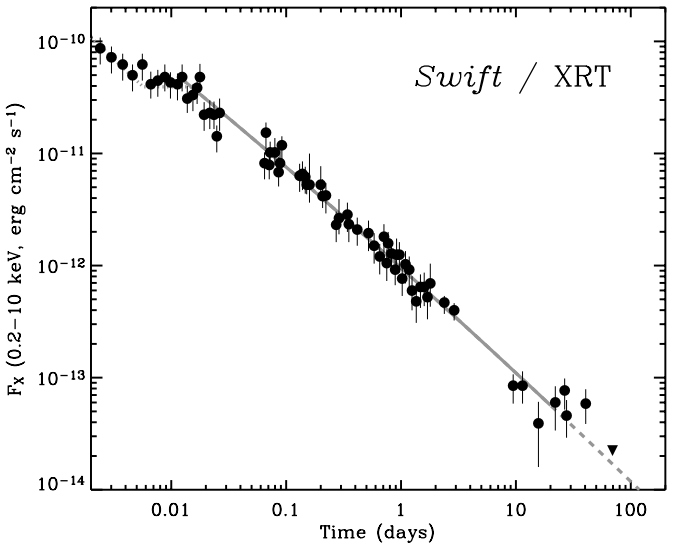

FIG. 7.—X-ray observations of XRF 050416a from the *Swift* XRT as reported by Mangano et al. (2007). The X-ray light curve is characterized by four phases: (1) an initial steep decay, (2) a flattening between $t \approx 0.005$ and 0.01 days, (3) a subsequent decay, and (4) a second flattening spanning $t \approx 20$–40 days. The final measurement at 70 days implies a rapid steepening following the second flattening. We attribute the late-time flattening to energy injection (refreshing shell or off-axis ejecta) or a large circumburst density jump. Overplotted is our afterglow model fit between 0.014 and 20 days (*solid gray line*) and extrapolated to late time (*dashed gray line*). We do not attempt to fit the data prior to 0.01 days (*dotted gray line*) due to insufficient broadband data.

(Rees & Mészáros 1998). We discuss each of these possibilities below.

4.1. *Off-Axis Jet Emission*

It has been shown that the observational signature of a relativistic jet viewed significantly away from our line of sight is a rapid achromatic rise in the early afterglow light curves (Paczyński 2001; Granot et al. 2002; Waxman 2004). In this scenario, the observed peak of the afterglow emission occurs as the spreading jet crosses our viewing angle. The timescale for this peak is $\sim$100 days for a GRB jet with typical parameters ($E_K = 10^{51}$ ergs, $n = 1$ cm^{-3}, $\epsilon_e = \epsilon_B = 0.1$, $\theta_j = 5^\circ$) viewed from an angle $\theta_{\rm obs} = 30^\circ$ (Soderberg et al. 2006b). The subsequent afterglow evolution is the same as that seen by an on-axis observer, decaying steeply with $\alpha = -p \approx -2$ to -3 for frequencies above ν_m (Sari et al. 1999). The observed timescale and evolution of the XRF 050416a radio flare are therefore roughly consistent with the predictions of an off-axis relativistic jet.

However, as noted by Mangano et al. (2007) and discussed in § 3.3, the early and steady decay of the XRF 050416a broadband afterglow implies the presence of relativistic ejecta directed along our line of sight. These ejecta are also responsible for the production of the observed prompt emission. Attributing the strong late-time radio flare to an energetic off-axis relativistic jet therefore implies that multiple relativistic ejecta components were produced in the explosion. Moreover, the steep rise and peak flux of the radio flare imply sharp edges for the off-axis jet and a kinetic energy 2–3 times larger than that of the on-axis ejecta. While this scenario cannot be ruled out, we consider it unlikely given the complicated ejecta geometry required.

4.1.1. *A Receding Jet*

Li & Song (2004) describe a related scenario in which a strong late-time radio flare is observed from a receding jet initially directed antiparallel to our line of sight. In this case, early afterglow emission is expected from the approaching jet, while emission from the receding jet is expected on a timescale $5t_{\rm NR}$ due to the light-travel time delay. This scenario is appealing in that it may explain both the early- and late-time afterglow emission observed for XRF 050416a within the standard framework of engine-driven (accretion-fed compact source; Piran 1999) double-sided jets. However, as discussed in § 3.3, broadband modeling of the afterglow emission predicts the nonrelativistic transition to occur no earlier than 0.6 yr, too late to explain the radio flare at 40 days. Moreover, the peak emission from a receding jet should be comparable to the radio flux at $t_{\rm NR}$ and decay with a temporal index given by the Sedov solution, $\alpha_{\rm rad} = -9/10$ (Li & Song 2004); both of these predictions are inconsistent with the observations. We conclude that afterglow emission from a receding jet is unlikely to produce the observed radio flare.

4.2. *Circumburst Density Variations*

It has been argued that abrupt variations in the circumburst medium can produce a strong rebrightening in the radio afterglows of GRBs. Specifically, the dynamical interaction of the forward shock with a wind termination shock at $r \sim 1$ pc is predicted to cause a rebrightening of the radio afterglow on a timescale of a few years (Wijers 2001; Ramirez-Ruiz et al. 2001, 2005). Here it is assumed that the blast wave is expanding nonrelativistically when it encounters the density jump, overall consistent with the observed timescales for nonrelativistic transitions (Frail et al. 2000, 2005; Berger et al. 2004). For comparison, the interaction of a relativistic blast wave with an abrupt (step function) density jump is not expected to cause strong variations in the afterglow light curves, where here it has been assumed that the postjump expansion is also relativistic (Nakar & Granot 2006).

In the case of XRF 050416a, the strong radio flare and X-ray plateau phase occur on a timescale when the blast wave is still relativistic, and therefore an abrupt circumburst density jump appears an unlikely explanation. This is supported by the fact that during the relativistic regime, the flux at frequencies above ν_c should be unaffected by circumburst density variations (Granot & Sari 2002). We speculate, however, that a very large density jump may be able to decelerate the blast wave to nonrelativistic speeds on a very short timescale and may therefore be able to explain the unusual late-time afterglow evolution. The increase in density would cause a shift in ν_a, which may explain the peculiar evolution of the spectral index in the radio band (Fig. 6). Based on our afterglow modeling (§ 3.2), we estimate that the circumburst radius of the forward shock at the onset of the radio flare was $\sim$1 pc, roughly consistent with the radius of a wind termination shock (Garcia-Segura et al. 1996; Chevalier et al. 2004). In this scenario, we expect a postjump self-similar evolution consistent with the Sedov-Taylor solution. Since the late-time radio and X-ray data are not sufficiently sensitive to trace the postflare evolution, we cannot rule out this possibility.

Finally, we investigated a scenario where the radio/X-ray flare is produced by the dynamical interaction of the quasi-spherical, nonrelativistic SN ejecta with a circumstellar medium (CSM) density enhancement. In fact, density jumps have been invoked to explain radio modulations observed for local (nonrelativistic) SNe Ibc (e.g., SN 2003bg; Soderberg et al. 2006a). Adopting a simple minimum energy calculation (Kulkarni et al. 1998) and requiring that the shock energy is equally partitioned between magnetic fields and relativistic electrons, we find that attributing the strong radio emission to the quasi-spherical SN component

requires that the SN ejecta is relativistic ($\Gamma \sim 10$) at the time of the radio/X-ray flare. However, as discussed above, strong flux variations are not expected while the blast wave is relativistic. Combined with the fact that the flare is at least a factor of 10^2 more radio luminous than any other SN Ibc ever observed (including GRB SN 1998bw; Kulkarni et al. 1998), we conclude that the radio/X-ray flare cannot be attributed to the quasi-spherical SN ejecta.

4.3. *Energy Injection*

An episode of energy injection may also cause a rebrightening of the afterglow flux. Energy injection may arise from long-lived central engine activity or under the framework of a "refreshed" shock where a slow moving shell ejected during the initial burst eventually catches up with the afterglow shock (Rees & Mészáros 1998; Granot et al. 2003). The observed ratio of the settling time to the epoch of injection, $\delta t/t$, can distinguish between these two scenarios. For $\delta t/t < 1$ the injection is produced by engine activity, while $\delta t/t \gtrsim 1$ indicates a refreshed shock. In the case of XRF 050416a, the X-ray and radio data after 20 days imply $\delta t/t > 1$, suggesting that the ejecta were refreshed on this timescale.

As shown in Figure 6, an extrapolation of the early radio evolution lies a factor of $\sim$3 below the observed flux at the onset of the radio flare. An energy increase affects the spectral parameters according to the following scalings: $\nu_a \propto E_{K,\rm iso}^{1/5}$, $\nu_m \propto E_{K,\rm iso}^{1/2}$, $F_{\nu_m} \propto E_{K,\rm iso}$, and $\nu_c \propto E_{K,\rm iso}^{-1/2}$ (Granot & Sari 2002). Given that ν_m is within the radio band on this timescale, we have $F_{\nu,\rm rad} \propto E_{K,\rm iso}$ and thus the radio flare corresponds to an energy injection of a comparable factor, $\sim$3. For the X-ray band, $F_{\nu,\rm X} \propto E_{K,\rm iso}^{(p+2)/4}$; thus, for $p \approx 2.1$ an energy injection of a factor of $\sim$3 corresponds to a comparable increase in the X-ray flux. The *Swift* XRT observations suggest a flattening on this timescale. Here we adopt the conservative assumption that the shock microphysics (ϵ_e, ϵ_B, and p) does not evolve during the energy injection.

One important implication of the energy injection model is that the postinjection asymptotic temporal decay should be the same as that before the injection. This prediction is consistent with the energy injection episodes invoked for GRB 021004 and GRB 030329 (Björnsson et al. 2004; Granot et al. 2003). However, in the case of XRF 050416a, the late-time radio and X-ray data suggest a steep postinjection decay, $\alpha \gtrsim -2$, significantly steeper than that observed preinjection. Moreover, the afterglow should asymptotically approach a flux normalization larger by a factor of $\sim$3 in both the radio and X-ray bands. As shown in Figures 6 and 7, this appears inconsistent with the observations, which suggest that the late-time afterglow is comparable to (or fainter than) an extrapolation of the early afterglow model. We note, however, that the faintness of the late-time afterglow and the steep postinjection decay may be explained if a jet break occurred on roughly the same timescale as the energy injection.

In comparison with other late-time afterglow studies (Frail et al. 2000, 2005; Tiengo et al. 2003; Berger et al. 2004; Kouveliotou et al. 2004), the radio flare and X-ray flattening observed for XRF 050416a are clearly atypical for long-duration GRBs. We therefore attribute the observed evolution to an unusual scenario involving either a large circumburst density jump or a late-time injection of energy (from a slow shell or off-axis ejecta).

4.4. *An Associated Supernova*

The *HST* measurements at late time can be used to constrain any possible contribution from an associated SN. Based on previous studies of GRB SNe, the thermal emission from an associated SN is predicted to reach maximum light on a timescale of $20(1+z)$ days with a peak magnitude of $M_{V,\rm rest} \approx -20$ mag or fainter (Zeh et al. 2004; Soderberg et al. 2006c and references therein). Observationally, the emergence of an SN component produces a steepening of the optical spectrum as the SN nears maximum light and dominates the afterglow emission.

An extrapolation of the broadband afterglow model to 40 days shows that the *HST* data are brighter by a factor of $\sim$5. For comparison, the radio flare and X-ray plateau on this same timescale represent flux density enhancements by factors of $\sim$3 and $\sim$2, respectively.

As discussed in § 2.2, we measure the spectrum of the optical transient within the ACS bands and find $\beta_{HST} \approx -2.8 \pm 0.3$ at 37 days. After correction for extinction (see § 2.1), the implied spectral index becomes $\beta_{HST} \approx -1.9$. For comparison, the spectral index between the radio and X-ray bands on this timescale (coincident with the radio flare and X-ray flattening) is $\beta_{\rm rad,X} \approx -0.56 \pm 0.04$, and the indices within the bands are $\beta_{\rm rad} \approx -0.6 \pm 0.2$ (Fig. 6) and $\beta_{\rm X} \approx -1.0$ (Mangano et al. 2007), respectively. Given that the *HST*-derived spectral index, even after correction for extinction, is (1) significantly steeper than the NIR/optical index observed at early time, $\beta_{\rm NIR/opt} \approx -1.4$, (2) significantly steeper than $\beta_{\rm rad,X}$ measured at a comparable epoch, and (3) inconsistent with the range of synchrotron spectral indices predicted for a relativistic blast wave ($\beta = [-1.5, 2.5]$; Sari et al. 1998), we conclude that the optical flux at $t \sim 40$ days is dominated by another emission process, likely an associated SN.

Next, to determine if the late-time optical data are consistent with the temporal evolution of a typical GRB/XRF-associated SN, we compare the *HST* flux values with synthesized SN light curves. We compiled *UBVRIJHK* observations of SN 1998bw from the literature (Galama et al. 1998; McKenzie & Schaefer 1999; Patat et al. 2001) and smoothed the extinction-corrected [Galactic component of $E(B-V) = 0.059$; Schlegel et al. 1998] light curves. Here we assume that the SN 1998bw host galaxy extinction is negligible, consistent with the findings of Patat et al. (2001) based on a spectroscopic analysis of the host galaxy. We then produced *k*-corrected NIR/optical light curves of SN 1998bw at the redshift of XRF 050416a by interpolating over the photometric spectrum and stretching the arrival time of the photons by a factor of $(1+z)$.

Shown in Figure 2 are the synthesized light curves for SN 1998bw at $z = 0.6528$, summed together with the afterglow model. The *HST* data are roughly comparable with the flux normalization and evolution of the summed model. Therefore, the temporal and spectral properties of the *HST* data suggest that XRF 050416a was associated with an SN similar to SN 1998bw. However, we caution that the temporal coincidence of the SN peak with the radio flare makes it difficult to estimate the relative contributions of the SN and afterglow.

5. HOST GALAXY PROPERTIES

We now turn to the properties of the GRB host galaxy. We measure the brightness of the host galaxy in the final *HST* epoch to be F775W $= 23.1 \pm 0.1$ mag ($I = 22.7 \pm 0.1$ mag). These values are not corrected for extinction. At $z = 0.6528$ the rest-frame *B* band is traced by the observed F775W band, leading to an absolute magnitude, $M_B \approx -20.3 \pm 0.1$ mag, or a luminosity $L_B \approx 0.5L^*$. This host luminosity is similar to that inferred for XRF 030528 (Rau et al. 2005) and the hosts of typical GRBs (Le Floc'h et al. 2003). At $z = 0.6528$, the measured offset of the optical transient (§ 2.1) relative to the center of the host galaxy corresponds to 140 ± 140 pc. This offset is a factor of $\sim$10

smaller than the median value for long-duration GRBs (Bloom et al. 2002).

As shown in Figure 5, the host exhibits several emission lines typical of star-forming galaxies. We estimate the star formation rate (SFR) in the host galaxy from the observed fluxes of the various emission lines. Using the flux of the [O II] λ3727 line, $F_{[O\,II]} \approx 9.6 \times 10^{-17}$ ergs cm^{-2} s^{-1} (Table 3), and the conversion of Kennicutt (1998), SFR $= (1.4 \pm 0.4) \times 10^{-41} L_{[O\,II]}\ M_\odot$ yr^{-1}, we find an SFR of about $2.5 \pm 0.7\ M_\odot$ yr^{-1}. From the Hβ line flux, $F_{H\beta} \approx 3.7 \times 10^{-17}$ ergs cm^{-2} s^{-1}, and assuming the case B recombination ratio of $F_{H\alpha}/F_{H\beta} = 2.87$ and the conversion of Kennicutt (1998), we infer an SFR of SFR $= 7.9 \times 10^{-42} L_{H\alpha} \approx 1.5 \pm 0.2\ M_\odot$ yr^{-1}. Thus, we conclude that the SFR (not corrected for extinction) is roughly $2\ M_\odot$ yr^{-1}. We note that the observed ratio of Hγ/H$\beta = 0.3 \pm 0.1$ compared to the theoretical value of about 0.47 (Osterbrock 1989) suggests a significant extinction correction (factor of $\sim$10) following the method of Calzetti et al. (1994). We conclude that the SFR for the host of XRF 050416a is similar to those inferred for long-duration GRBs (Christensen et al. 2004; Berger et al. 2003a) and at least an order of magnitude larger than that inferred for XRF 020903 (Soderberg et al. 2004a; Bersier et al. 2006).

The combination of the inferred SFR and host luminosity provides a measure of the specific SFR. We find a value of $4\ M_\odot$ yr$^{-1}(L^*/L)$ (uncorrected for extinction), which is about a factor of 2 lower than the mean specific SFR for the hosts of long-duration GRBs (Christensen et al. 2004).

Next, we use the relative strengths of the oxygen and hydrogen emission lines to infer the ionization state and oxygen abundance. The relevant indicators are $R_{23} \equiv \log(F_{[O\,II]} + F_{[O\,III]}/F_{H\beta}) \approx 0.74$ and $O_{32} \equiv \log(F_{[O\,III]}/F_{[O\,II]}) \approx 0.055$. Using the calibrations of McGaugh (1991) and Kobulnicky & Kewley (2004), we find that for the upper branch the metallicity is $12 + \log(O/H) \approx 8.6$ while for the lower branch it is about 7.9; the two branches are due to the double-valued nature of R_{23} in terms of metallicity. Thus, the host metallicity of XRF 050416a is 0.2–0.8 $Z_\odot$, larger than that inferred for XRF 060218 (Modjaz et al. 2006; Wiersema et al. 2007) and comparable to that for XRF 030528 (Rau et al. 2005). Moreover, this range is somewhat higher than the typical metallicities for GRB hosts, some of which have metallicities that are $\sim$1/10 solar (e.g., Prochaska et al. 2006).

6. IS XRF 050416a A SHORT BURST?

With a prompt emission duration of just $T_{90} \approx 2.4$ s (Sakamoto et al. 2006a), it is interesting to consider XRF 050416a as a member of the short-hard class of GRBs, popularly believed to result from the coalescence of neutron stars or black holes (e.g., Eichler et al. 1989). Based on the bimodal BATSE duration distribution, bursts with $T_{90} \gtrsim 2$ s are assumed to belong to the long-duration class (Kouveliotou et al. 1993), although a decomposition of the overlapping distributions suggests that a small fraction of SHBs have durations longer than this cutoff. The distinction between short-hard and long-duration bursts is further complicated by the detection of soft X-ray tails lasting several seconds following SHB 050709 and SHB 050724 (Villasenor et al. 2005; Barthelmy et al. 2005). This suggests that SHBs are not necessarily characterized by a pure hard emission spectrum (Sakamoto et al. 2006b). Related to this issue is the use of spectral lags to distinguish between long and short bursts. As discussed by Norris & Bonnell (2006), long-duration bursts typically have longer lags that correlate with isotropic-equivalent prompt gamma-ray luminosity (Norris et al. 2000). On the other hand, SHBs have negligible (or even negative) spectral lags.

In the case of XRF 050416a, the prompt duration places it between the long- and short-duration classes. The low value of E_p may suggest that it belongs to the long-duration class; however, it is becoming clear that hardness cannot be used to reliably distinguish between the two classes (for further discussion see Nakar 2007). Similarly, while the negative lag inferred for XRF 050416a may suggest an SHB classification, examples do exist of long-duration BATSE bursts with negative lags (Norris & Bonnell 2006).

Afterglow modeling may provide additional clues. The range of values we infer for the XRF 050416a beaming-corrected energies are overall consistent with those of long-duration GRBs, including the subclass of subenergetic bursts. At the same time, they are roughly consistent with the values inferred for SHBs (Fox et al. 2005; Berger et al. 2005; Soderberg et al. 2006d). However, the low circumburst density, $n \sim 10^{-3}$, is a factor of 10–10^4 smaller than the typical values inferred for long-duration GRBs (e.g., Panaitescu & Kumar 2002; Yost et al. 2003; Chevalier et al. 2004) but comparable to those of SHBs (Fox et al. 2005; Berger et al. 2005; Bloom et al. 2006; Burrows et al. 2006; Panaitescu 2006; Soderberg et al. 2006d). The observed radio flare and X-ray flattening at 20 days are atypical for both long- and short-duration GRBs and therefore cannot be used to classify this event. However, it is interesting to note that large variations in the circumburst density are more naturally explained in the context of a massive stellar progenitor with interacting stellar winds (Garcia-Segura et al. 1996; Ramirez-Ruiz et al. 2001).

Next is a discussion of the XRF 050416a host galaxy, since long- and short-duration bursts may also be distinguished by their environments (for a recent review see Berger 2006). As discussed in § 5, the host is a star-forming galaxy with an inferred SFR and metallicity comparable to those of long-duration GRBs. Moreover, XRF 050416a is located near the center and brightest part of its host galaxy. It is thus consistent with the locations of long-duration bursts with respect to their hosts (Bloom et al. 2002; Fruchter et al. 2006). For comparison, SHBs are typically localized to low SFR hosts with significant old stellar populations at radial offsets up to a factor of 10 larger than those of typical long-duration bursts (Berger et al. 2005; Fox et al. 2005; Bloom et al. 2007; Soderberg et al. 2006d).

Finally, the discovery of an associated Type Ic SN is perhaps one of the best methods to distinguish between long- and short-duration bursts. The discovery of several long-duration bursts and X-ray flashes at $z \lesssim 0.3$ in the last few years has firmly established that GRBs and XRFs are accompanied by SNe of Type Ic (Galama et al. 1998; Stanek et al. 2003; Malesani et al. 2004; Soderberg et al. 2005; Pian et al. 2006). A study of the luminosity distribution for GRB/XRF SNe reveals a significant dispersion, implying a spread of (at least) an order of magnitude in peak optical luminosity (Zeh et al. 2004; Soderberg et al. 2006c). At the same time, deep imaging of SHBs has constrained any associated SN emission to be up to $\sim$100 times less luminous than SN 1998bw (Fox et al. 2005; Soderberg et al. 2006d). In the case of XRF 050416a, the temporal and spectral properties of the *HST* data suggest that XRF 050416a was accompanied by an SN with a peak luminosity roughly similar to SN 1998bw. We stress, however, that the temporal coincidence of the radio flare with the SN peak complicates any study of the SN properties.

Based on the associated SN and large-scale environmental properties, we conclude that XRF 050416a is a member of the long-duration class of GRBs. This event highlights the difficulty in classifying bursts based on their prompt emission properties alone.

7. DISCUSSION AND CONCLUSIONS

We present extensive broadband NIR/optical and radio data for the afterglow of the X-ray flash XRF 050416a and show that it is localized to a star-forming ($\gtrsim 2\ M_\odot\ \mathrm{yr}^{-1}$) host galaxy at $z = 0.6528$. Along with XRF 020903, XRF 030723, and XRF 060218, this burst is one of the best-studied X-ray flashes to date. Moreover, XRF 050416a is only the third XRF with a spectroscopic redshift for which a broadband afterglow study has been performed and the physical parameters have been constrained. The isotropic-equivalent prompt and kinetic energy releases are $E_{\gamma,\mathrm{iso}} \approx 1.2 \times 10^{51}$ ergs (Sakamoto et al. 2006a) and $E_{K,\mathrm{iso}} \approx 10^{52}$ ergs, respectively. These values are 10^2 times larger than those of XRF 020903 (Sakamoto et al. 2004; Soderberg et al. 2004a) and up to 10^4 times larger than those inferred for subenergetic GRB 980425, GRB 031203, and XRF 060218 (Pian et al. 2000; Kulkarni et al. 1998; Sazonov et al. 2004; Soderberg et al. 2004b, 2006e; Campana et al. 2006).

Adopting the results of our standard synchrotron model and $t_j \gtrsim 20$ days, we constrain the collimation of the ejecta to $\theta_j \gtrsim 6.9^\circ$–$9.7^\circ$, slightly larger than the median value of 5° for typical GRBs (Bloom et al. 2003b; Ghirlanda et al. 2004 and references therein). This indicates that the beaming-corrected energy release is $E_K \approx 9.8 \times 10^{49}$–$1.4 \times 10^{52}$ ergs and $E_\gamma \approx 8.6 \times 10^{48}$–$1.2 \times 10^{51}$ ergs, implying a total relativistic energy yield of $E_{\mathrm{tot}} \approx 1.1 \times 10^{50}$–$1.5 \times 10^{52}$ ergs, which straddles the median value for cosmological GRBs, $E_{\mathrm{tot}} \approx 2 \times 10^{51}$ ergs (Berger et al. 2003c). However, the efficiency in converting the energy in the ejecta into gamma rays is $\eta_\gamma \equiv E_\gamma/(E_K + E_\gamma) \approx 0.04$–$0.08$, significantly lower than the typical values for GRBs (Panaitescu & Kumar 2002; Yost et al. 2003) and comparable to that inferred for XRF 020903 ($\eta_\gamma \approx 0.03$; Soderberg et al. 2004a). This strengthens the idea that XRFs and GRBs are distinguished by their ability to couple significant energy to highly relativistic material (Soderberg et al. 2004a; Zhang et al. 2004).

In addition to the burst energetics, several key results emerge from our broadband analysis of XRF 050416a. First is the detection of a bright, late-time radio flare accompanied by an observed flattening in the X-ray bands that we attribute to a large circumburst density enhancement or episode of energy injection (refreshing shell or off-axis ejecta) at $t \sim 20$ days. In the context of a density jump, it is interesting to note that the inferred prejump circumburst density is several orders of magnitude lower than the values typically inferred for long-duration GRBs (for a recent compilation see Soderberg et al. 2006b). Moreover, radio observations of local (optically selected) core-collapse SNe show similar flux modulations (factor of 2–3) attributed to abrupt variations in the CSM (Weiler et al. 1991; Ryder et al. 2004; Soderberg et al. 2006a).

Next, the temporal and spectral evolution of the optical afterglow suggests the contribution from an SN component with peak luminosity and light-curve shape comparable to SN 1998bw. Given the temporal coincidence of the radio flare and X-ray flattening with the SN peak, XRF 050416a highlights the need for full spectral coverage in late-time GRB/XRF SN searches. This is illustrated by the optical rebrightening observed for XRF 030723 at $\sim$15 days and interpreted as a thermal SN component (Fynbo et al. 2004), while the X-ray and radio data show similar rebrightenings at late-time suggesting a CSM density jump or energy injection (Butler et al. 2005; A. M. Soderberg et al. 2007, in preparation).

With the addition of XRF 050416a, there are three XRFs (XRF 020903, XRF 060218, and now XRF 050416a) with spectroscopic redshifts observed in association with SNe with peak luminosities varying by up to a factor of 10 compared to SN 1998bw (Soderberg et al. 2005; Bersier et al. 2006; Pian et al. 2006). However, deep *HST* observations of XRF 040701 at $z = 0.21$ revealed that any associated SN was at least 10 (and likely $\gtrsim$100) times fainter than SN 1998bw (Soderberg et al. 2005). It is therefore clear that most XRFs produce nickel-rich SN explosions, but that there is a significant dispersion in the peak luminosities of XRF-associated SNe. A similar result is found for GRB-associated SNe (Zeh et al. 2004; Soderberg et al. 2006c) and further strengthens the idea that GRBs and XRFs are intimately related.

Finally, we address XRF 050416a within the framework of off-axis and dirty fireball models for XRFs. As discussed in § 3.3, the evolution of the early afterglow indicates that the ejecta are being viewed along the collimation axis. Similarly, on-axis viewing angles are inferred from afterglow studies of XRF 020903 (Soderberg et al. 2004a), XRF 050215B (Levan et al. 2006), XRF 050406 (Romano et al. 2006), and XRF 060218 (Campana et al. 2006; Soderberg et al. 2006e). Unification models in which X-ray flashes are understood as typical GRBs viewed away from the burst collimation axis (e.g., Granot et al. 2002; Yamazaki et al. 2003) are therefore inconsistent with the observations for these five events. To date, such models are only consistent with the observations of one X-ray flash: XRF 030723 (Fynbo et al. 2004; Butler et al. 2005; Granot et al. 2005).

While the lack of high-energy photons prevents a direct constraint on the Lorentz factor of the burst, our detailed afterglow modeling allows us to place a lower limit on the initial bulk Lorentz factor, $\Gamma_0 \gtrsim 110$, by extrapolating $\Gamma \propto t^{-3/8}$ back to the first XRT observation at $\sim$100 s. This value is somewhat lower than the typical values inferred for cosmological GRBs (Panaitescu & Kumar 2002) and consistent with the upper range of values predicted for a dirty fireball. Given that some dirty fireball models predict XRFs to have wider jets than typical GRBs (e.g., Zhang et al. 2003), it is interesting to note that there are no X-ray flashes for which an achromatic jet break has been observed. This may suggest that their ejecta are not strongly collimated. In fact, detailed radio observations of XRF 020903 and XRF 060218 spanning $\gtrsim$100 days imply a quasi-spherical ejecta geometry in both cases (Soderberg et al. 2004a, 2006e).

While the basic properties of X-ray flashes (redshifts, hosts, isotropic gamma-ray energies) are now available for several events, it is clear that broadband afterglow observations are required for a complete understanding of the burst properties. With the addition of XRF 050416a to the existing sample of only a few well-studied events, we continue to work toward a systematic comparison of the global characteristics of XRFs and GRBs. While limited, the current sample suggests that the two classes share similar ejecta energies, associated SNe, and viewing angles. Further studies of XRF afterglows will be used to confirm whether the two classes differ in their collimation angles.

The authors thank Re'em Sari and Don Lamb for helpful discussions. As always, the authors thank Jochen Greiner for maintaining his GRB page. A. M. S. and S. B. C. are supported by the NASA Graduate Student Research Program. E. B. and A. G. acknowledge support by NASA through Hubble Fellowship grants awarded by STScI, which is operated by AURA, Inc., for NASA. GRB research at Caltech is supported through NASA.

REFERENCES

Alard, C. 2000, A&AS, 144, 363
Amati, L. 2006, MNRAS, 372, 233
Band, D., et al. 1993, ApJ, 413, 281
Barthelmy, S. D., et al. 2005, Nature, 438, 994
Berger, E. 2006, in AIP Conf. Proc. 836, Gamma-Ray Bursts in the Swift Era, ed. S. S. Holt, N. Gehrels, & J. A. Nousek (New York: AIP), 33
Berger, E., Cowie, L. L., Kulkarni, S. R., Frail, D. A., Aussel, H., & Barger, A. J. 2003a, ApJ, 588, 99
Berger, E., Kulkarni, S. R., & Frail, D. A. 2003b, ApJ, 590, 379
———. 2004, ApJ, 612, 966
Berger, E., et al. 2003c, Nature, 426, 154
———. 2005, Nature, 438, 988
Bersier, D., et al. 2006, ApJ, 643, 284
Björnsson, G., Gudmundsson, E. H., & Jóhannesson, G. 2004, ApJ, 615, L77
Bloom, J. S., Fox, D., van Dokkum, P. G., Kulkarni, S. R., Berger, E., Djorgovski, S. G., & Frail, D. A. 2003a, ApJ, 599, 957
Bloom, J. S., Frail, D. A., & Kulkarni, S. R. 2003b, ApJ, 594, 674
Bloom, J. S., Kulkarni, S. R., & Djorgovski, S. G. 2002, AJ, 123, 1111
Bloom, J. S., et al. 2006, ApJ, 638, 354
———. 2007, ApJ, 654, 878
Burrows, D. N., et al. 2006, ApJ, 653, 468
Butler, N. R., et al. 2005, ApJ, 621, 884
Calzetti, D., Kinney, A. L., & Storchi-Bergmann, T. 1994, ApJ, 429, 582
Campana, S., et al. 2006, Nature, 442, 1008
Chevalier, R. A., Li, Z.-Y., & Fransson, C. 2004, ApJ, 606, 369
Christensen, L., Hjorth, J., & Gorosabel, J. 2004, A&A, 425, 913
Dermer, C. D., Chiang, J., & Böttcher, M. 1999, ApJ, 513, 656
Eichler, D., Livio, M., Piran, T., & Schramm, D. N. 1989, Nature, 340, 126
Fox, D. B., et al. 2005, Nature, 437, 845
Frail, D. A., Kulkarni, S. R., Berger, E., & Wieringa, M. H. 2003, AJ, 125, 2299
Frail, D. A., Soderberg, A. M., Kulkarni, S. R., Berger, E., Yost, S., Fox, D. W., & Harrison, F. A. 2005, ApJ, 619, 994
Frail, D. A., Waxman, E., & Kulkarni, S. R. 2000, ApJ, 537, 191
Frail, D. A., et al. 2001, ApJ, 562, L55
Freedman, D. L., & Waxman, E. 2001, ApJ, 547, 922
Fruchter, A. S., & Hook, R. N. 2002, PASP, 114, 144
Fruchter, A. S., et al. 2006, Nature, 441, 463
Fynbo, J. P. U., et al. 2004, ApJ, 609, 962
Galama, T. J., & Wijers, R. A. M. J. 2001, ApJ, 549, L209
Galama, T. J., et al. 1998, Nature, 395, 670
Garcia-Segura, G., Langer, N., & Mac Low, M.-M. 1996, A&A, 316, 133
Ghirlanda, G., Ghisellini, G., & Lazzati, D. 2004, ApJ, 616, 331
Granot, J., Nakar, E., & Piran, T. 2003, Nature, 426, 138
Granot, J., Panaitescu, A., Kumar, P., & Woosley, S. E. 2002, ApJ, 570, L61
Granot, J., Ramirez-Ruiz, E., & Perna, R. 2005, ApJ, 630, 1003
Granot, J., & Sari, R. 2002, ApJ, 568, 820
Heise, J., in't Zand, J., Kippen, R. M., & Woods, P. M. 2001, in Gamma-Ray Bursts in the Afterglow Era, ed. E. Costa, F. Frontera, & J. Hjorth (Berlin: Springer), 16
Henden, A. 2005, GRB Circ. 3454, http://gcn.gsfc.nasa.gov/gcn/gcn3/3454.gcn3
Holland, S. T., et al. 2007, AJ, 133, 122
Jakobsson, P., et al. 2004, A&A, 427, 785
Kennicutt, R. C., Jr. 1998, ARA&A, 36, 189
Kobulnicky, H. A., & Kewley, L. J. 2004, ApJ, 617, 240
Kouveliotou, C., Meegan, C. A., Fishman, G. J., Bhat, N. P., Briggs, M. S., Koshut, T. M., Paciesas, W. S., & Pendleton, G. N. 1993, ApJ, 413, L101
Kouveliotou, C., et al. 2004, ApJ, 608, 872
Kulkarni, S. R., et al. 1998, Nature, 395, 663
———. 1999, ApJ, 522, L97
Le Floc'h, E., et al. 2003, A&A, 400, 499
Levan, A. J., et al. 2006, ApJ, 648, 1132
Li, W., Chornock, R., Jha, S., & Filippenko, A. V. 2005, GRB Circ. 3270, http://gcn.gsfc.nasa.gov/gcn/gcn3/3270.gcn3
Li, Z., & Song, L. M. 2004, ApJ, 614, L17
Lithwick, Y., & Sari, R. 2001, ApJ, 555, 540
Livio, M., & Waxman, E. 2000, ApJ, 538, 187
Malesani, D., et al. 2004, ApJ, 609, L5
Mangano, V., et al. 2007, ApJ, 654, 403
McGaugh, S. S. 1991, ApJ, 380, 140
McKenzie, E. H., & Schaefer, B. E. 1999, PASP, 111, 964
Mirabal, N., Halpern, J. P., An, D., Thorstensen, J. R., & Terndrup, D. M. 2006, ApJ, 643, L99
Modjaz, M., et al. 2006, ApJ, 645, L21
Nakar, E. 2007, Phys. Rep., in press (astro-ph/0701748)
Nakar, E., & Granot, J. 2006, preprint (astro-ph/0606011)
Norris, J. P., & Bonnell, J. T. 2006, ApJ, 643, 266
Norris, J. P., Marani, G. F., & Bonnell, J. T. 2000, ApJ, 534, 248
Nousek, J. A., et al. 2006, ApJ, 642, 389
O'Brien, P. T., et al. 2006, ApJ, 647, 1213
Osterbrock, D. E. 1989, Astrophysics of Gaseous Nebulae and Active Galactic Nuclei (Mill Valley: University Science Books)
Paczyński, B. 2001, Acta Astron., 51, 1
Panaitescu, A. 2006, MNRAS, 367, L42
Panaitescu, A., & Kumar, P. 2002, ApJ, 571, 779
Patat, F., et al. 2001, ApJ, 555, 900
Pei, Y. C. 1992, ApJ, 395, 130
Pian, E., et al. 2000, ApJ, 536, 778
———. 2006, Nature, 442, 1011
Piran, T. 1999, Phys. Rep., 314, 575
Predehl, P., & Schmitt, J. H. M. M. 1995, A&A, 293, 889
Price, P. A., Minezaki, T., Cowie, L., & Yoshii, Y. 2005, GRB Circ. 3312, http://gcn.gsfc.nasa.gov/gcn/gcn3/3312.gcn3
Prochaska, J. X., et al. 2006, ApJ, 642, 989
Qiu, Y., Lu, C. L., Lou, Y. Q., Huang, K. Y., & Urata, Y. 2005, GRB Circ. 3286, http://gcn.gsfc.nasa.gov/gcn/gcn3/3286.gcn3
Ramirez-Ruiz, E., Dray, L. M., Madau, P., & Tout, C. A. 2001, MNRAS, 327, 829
Ramirez-Ruiz, E., García-Segura, G., Salmonson, J. D., & Pérez-Rendón, B. 2005, ApJ, 631, 435
Rau, A., Salvato, M., & Greiner, J. 2005, A&A, 444, 425
Rees, M. J., & Mészáros, P. 1998, ApJ, 496, L1
Romano, P., et al. 2006, A&A, 450, 59
Ryder, S. D., Sadler, E. M., Subrahmanyan, R., Weiler, K. W., Panagia, N., & Stockdale, C. 2004, MNRAS, 349, 1093
Sakamoto, T., et al. 2004, ApJ, 602, 875
———. 2005, ApJ, 629, 311
———. 2006a, ApJ, 636, L73
———. 2006b, in AIP Conf. Proc. 836, Gamma-Ray Bursts in the Swift Era, ed. S. S. Holt, N. Gehrels, & J. A. Nousek (New York: AIP), 43
Sari, R., & Piran, T. 1999, ApJ, 517, L109
Sari, R., Piran, T., & Halpern, J. P. 1999, ApJ, 519, L17
Sari, R., Piran, T., & Narayan, R. 1998, ApJ, 497, L17
Sazonov, S. Y., Lutovinov, A. A., & Sunyaev, R. A. 2004, Nature, 430, 646
Schady, P., et al. 2006, ApJ, 643, 276
Schlegel, D. J., Finkbeiner, D. P., & Davis, M. 1998, ApJ, 500, 525
Sirianni, M., et al. 2005, PASP, 117, 1049
Smith, J. A., et al. 2002, AJ, 123, 2121
Soderberg, A. M. 2006, in AIP Conf. Proc. 836, Gamma-Ray Bursts in the Swift Era, ed. S. S. Holt, N. Gehrels, & J. A. Nousek (New York: AIP), 380
Soderberg, A. M., Chevalier, R. A., Kulkarni, S. R., & Frail, D. A. 2006a, ApJ, 651, 1005
Soderberg, A. M., Nakar, E., Berger, E., & Kulkarni, S. R. 2006b, ApJ, 638, 930
Soderberg, A. M., et al. 2004a, ApJ, 606, 994
———. 2004b, Nature, 430, 648
———. 2005, ApJ, 627, 877
———. 2006c, ApJ, 636, 391
———. 2006d, ApJ, 650, 261
———. 2006e, Nature, 442, 1014
Stanek, K. Z., et al. 2003, ApJ, 591, L17
Tiengo, A., Mereghetti, S., Ghisellini, G., Rossi, E., Ghirlanda, G., & Schartel, N. 2003, A&A, 409, 983
Torii, K. 2005, GRB Circ. 3272, http://gcn.gsfc.nasa.gov/gcn/gcn3/3272.gcn3
Villasenor, J. S., et al. 2005, Nature, 437, 855
Waxman, E. 2004, ApJ, 602, 886
Weiler, K. W., van Dyk, S. D., Discenna, J. L., Panagia, N., & Sramek, R. A. 1991, ApJ, 380, 161
Wiersema, K., et al. 2007, A&A, in press (astro-ph/0701034)
Wijers, R. A. M. J. 2001, in Gamma-Ray Bursts in the Afterglow Era, ed. E. Costa, F. Frontera, & J. Hjorth (Berlin: Springer), 306
Yamazaki, R., Yonetoku, D., & Nakamura, T. 2003, ApJ, 594, L79
Yanagisawa, K., Toda, H., & Kawai, N. 2005, GRB Circ. 3287, http://gcn.gsfc.nasa.gov/gcn/gcn3/3287.gcn3
Yost, S. A., Harrison, F. A., Sari, R., & Frail, D. A. 2003, ApJ, 597, 459
Zeh, A., Klose, S., & Hartmann, D. H. 2004, ApJ, 609, 952
Zel'dovich, Y. B., & Raizer, Y. P. 2002, Physics of Shock Waves and High Temperature Hydrodynamic Phenomena (Mineola: Dover)
Zhang, W., Woosley, S. E., & Heger, A. 2004, ApJ, 608, 365
Zhang, W., Woosley, S. E., & MacFadyen, A. I. 2003, ApJ, 586, 356